Journal of Materials Science & Technology 167 (2023) 82–93

Contents lists available at ScienceDirect

Journal of Materials Science & Technology

journal homepage: www.elsevier.com/locate/jmst

Research Article

# Engineering phosphorus-containing lignin for epoxy biocomposites with enhanced thermal stability, fire retardancy and mechanical properties

Anlin Zhang[a,1], Jianzhong Zhang[a,1], Lina Liu[a], Jinfeng Dai[a,*], Xinyu Lu[a], Siqi Huo[b,*], Min Hong[b], Xiaohuan Liu[c], Mark Lynch[d], Xuesen Zeng[b], Paulomi Burey[b,d], Pingan Song[b,d,*]

[a] College of Chemistry and Materials Science, Zhejiang A&F University, Hangzhou 311300, China
[b] Centre for Future Materials, University of Southern Queensland, Springfield, QLD 4300, Australia
[c] College of Life Science, Zhejiang Provincial Key Laboratory of Plant Evolutionary Ecology and Conservation, Taizhou University, Taizhou 318000, China
[d] School of Agriculture and Environmental Science, University of Southern Queensland, Springfield, QLD 4300, Australia

ARTICLE INFO

*Article history:*
Received 24 April 2023
Revised 27 May 2023
Accepted 4 June 2023
Available online 22 June 2023

*Keywords:*
Epoxy resin
Lignin
Flame retardancy
Thermal stability
Mechanical property

ABSTRACT

Fabricating a high-performing thermoset using bio-based flame retardant is critical for the sustainable development of engineering materials with superior fire safety and robust mechanical properties. Herein, the epoxy (EP) composites with the industrial requirements are manufactured with a novel high-efficient, lignin-based flame retardant named DAL-*x*, which is fabricated by grafting 9, 10-dihydro-9-oxa-10-phosphaze-10-oxide (DOPO) onto lignin. The resulting DAL-*x*/EP composite exhibits excellent flame retardancy with a desirable UL-94 V-0 rating and a satisfactory limiting oxygen index (LOI) of 29.8% due to the appropriate phosphorus content of DAL-*x* with adjustable molecular chain structure. Moreover, the DAL-*x*/EP composite shows an unexpected improvement in the elastic modulus (~36%) and well-preserved strength and ductility compared with those of pure EP. This work offers a feasible strategy for creating efficient bio-based flame retardants utilizing industrial waste lignin and preparing high-performance EP composites that meet the demanding requirement of fire retardancy in industries, contributing to the circular economy and sustainability.



## 1. Introduction

Epoxy resins (EPs), as one of the most significantly versatile thermosetting materials, have been widely used in electronic and electrical appliances, aerospace, new energy vehicles, and other fields [1–5] due to their advantages of thermal stability [6–8], electrical insulation [9–11], and corrosion resistance [12–14]. However, EPs are inherently combustible and release heavy toxic smoke with large amounts of heat during burning, which may cause serious damage to human health and environment [15,16]. With the rapid development of electronic components, the EPs used in this field have been facing higher performance requirements, notably fire safety.

Recently, high-efficiency halogen flame retardants are problematic in industrial applications due to environmental concerns [17–20]. Therefore, phosphorous-containing flame retardants show promise as effective alternatives to halogen ones, benefiting from both their environmentally friendly and superior flame-retardant performance [21,22]. Among them, 9, 10-dihydro-9-oxa-10-phosphaze-10-oxide (DOPO) and its derivatives are currently employed as flame-retardants to improve the fire safety of EPs, due to multiple mechanisms of flame retardation [23–28]. For example, Jin et al. [29] synthesized a DOPO derivative (ABD) and applied it to EPs. With 3 wt.% of ABD, the resulting EP composite exhibited a high limiting oxygen index (LOI) of 36.5% and passed a UL-94 V-0 rating. Moreover, the cone calorimetry results further showed that the peak heat release rate (PHRR), total heat release (THR), and total smoke production (TSP) were greatly reduced after adding ABD, demonstrating the flame quenching and smoke suppression effects of ABD. Liu et al. [30] constructed a DOPO derivative (DPI) containing a rigid and flexible structure. With 4 wt.% of DPI present, the EP composite achieved a UL-94 V-0 rating and a high LOI value of

* Corresponding authors.
*E-mail addresses:* Jinfengdai0601@zafu.edu.cn (J. Dai), Siqi.Huo@usq.edu.au (S. Huo), pingansong@gmail.com, pingan.song@usq.edu.au (P. Song).
[1] These authors equally contributed to this work and are listed as co-first authors.

https://doi.org/10.1016/j.jmst.2023.06.004
1005-0302/

39.5%. Also, the mechanical properties of the EP composite with 4 wt.% DPI were greatly elevated. Thus, the reported DOPO-derived flame retardants show both superior flam-retardant performance and high efficiency towards EPs, but with the downside of being derived from petrochemical resources.

Lignin is the second most abundant organic material in nature with inherent aromatic structure and plentiful functional groups. Therefore, lignin is increasingly recognized as a potential candidate for the preparation of biomass flame retardant, based on its good thermal stability and charring capacity [31–33]. However, direct use of lignin in EP as a flame retardant is not satisfactory due to the lack of fire quenching and catalytic char formation [34–36]. Thus, it appears necessary to combine lignin with flame-retardant components, such as nitrogen-, phosphorus-, and silicon-containing groups, for it to realize its full potential as an efficient flame retardant in EPs [37–42]. For example, Lu et al. [43] synthesized a lignin-based flame retardant (Lig-F) using DOPO and piperazine (PA) as grafting agents. As a result, the LOI value of EP composite with 10 wt.% of Lig-F reached 34.8%, and the char residue at 800 °C increased to 20.7 wt.%. Alternately, Lu et al. [44] prepared a lignin-based liquid EP using lignin, phenol, and glyoxal through a chemical crosslinking reaction, and synthesized a bi-hydroxyl-bi-DOPO compound. The presence of 0.18 wt.% phosphorus content made the resulting EP pass a UL-94 V-0 rating with an LOI value of 35.2%. The heat release (including PHRR and THR) of the EP was also drastically decreased. Unfortunately, the above lignin-containing EP composites suffered from deteriorated mechanical properties because of the poor compatibility between matrix and additives, and the rigidity and weak reactivity of lignin hinders the curing process and reduces the crosslinking density.

Developing sustainable materials with high performance and fire safety for practical applications requires green multifunctional flame retardants with both efficient and eco-friendly based on renewable substrates. In this work, we aim to construct a green and efficient lignin-based flame retardant (DAL-*x*) by grafting DOPO into the lignin structure through polymerization without highly toxic organic solvents. The DAL-*x* consisting of hard lignin, soft polyallyl-methacrylate and flame retardant DOPO exhibits excellent fire resistance, enhancement, and smoke suppression, allowing the EP composites to achieve excellent fire safety properties with high-performing mechanical properties. We evaluated the influences of the as-prepared DAL-*x* on the thermal, combustion behaviors and mechanical properties of DAL-*x*/EP composites, and discussed the toughening and flame-retardant mechanisms of DAL-*x* in detail. This work may potentially usher in a new era of lignin-based flame retardants, by providing a feasible strategy for manufacturing bio-based, fire-safety thermosets. There is also a significant benefit in exploring a new green strategy for the value-added utilization of industrial waste lignin.

## 2. Experimental

### 2.1. Materials

Epoxy resin (E51) was supplied by Hangzhou Wuhuigang Adhesive Co., Ltd., China. Enzymatic hydrolysis lignin was purchased from Shandong Longli Technology Co., Ltd., China. Allyl methacrylate (AMA, 99%), dimethyl sulfoxide (DMSO, >99%), dimethylformamide (DMF, 99.5%), calcium chloride ($CaCl_2$, 99.5%), 9, 10-dihydro-9-oxygen-10-phosphate phenanthrene 10-oxide (DOPO, 97%), anhydrous ethanol (99.5%), 1,4-dioxane (99%) and 4,4′-diaminodiphenylmethane (99%) were bought from Shanghai Aladdin Biochemical Technology Co., Ltd., China. Hydrogen peroxide ($H_2O_2$, 30%) was obtained from Sinopharm Chemical Reagent Co., Ltd., China. All chemicals were used as received.

### 2.2. Synthesis of AL-x

Firstly, 28.4 mmol $CaCl_2$ was added into a 250 mL round-bottled flask containing 50 mL DMSO solution with magnetic stirring until their complete dissolution. Then, 0.8 mmol lignin was added into the solution. After lignin was completely dissolved, 12 mmol AMA and 38.7 nmol 30% $H_2O_2$ were added dropwise, and the reaction was magnetically stirred at 40 °C for 24 h. After that, the reaction solution was dropped slowly into deionized water, and the obtained precipitate was collected, and washed with deionized water 3 times. Finally, the solid sample was dried in a vacuum oven at 60 °C for 24 h and labeled as AL-1. Using the same reaction conditions, 24 and 36 mmol AMA was used to form the obtained solid samples, labeled as AL-2 and AL-3, respectively.

### 2.3. Synthesis of DAL-x

In a 250 mL round-bottomed flask, 20 mmol DOPO was dissolved in 50 mL DMF by magnetic stirring. Then, 0.4 mmol AL-1 was added and stirred until complete. The reaction was carried out at 150 °C for 9 h. The reaction solution was slowly dropped into deionized water. The precipitate was collected and washed with anhydrous ethanol 3 times. Finally, the solid sample was dried in a vacuum oven at 60 °C for 24 h, named DAL-1. Under the same reaction conditions, AL-1 was replaced by AL-2 or AL-3, with the obtained solid sample labeled DAL-2 or DAL-3 respectively.

### 2.4. Preparation of DAL-x/EP composites

The flame-retardant EP thermosets containing 5 wt.%, 7.5 wt.% and 10 wt.% of DAL-*x* were prepared using DDM as a curing agent, and all epoxy composites were denoted as 10DAL-1/EP, 10DAL-2/EP, 10DAL-3/EP, 7.5DAL-3/EP, and 5DAL-3/EP. Besides, the neat EP and EP thermosets containing 10 wt.% AL-3 or 2 wt.% DOPO were fabricated as the control samples, and named as EP, 10AL-3/EP and 2DOPO/EP.

The detailed EP thermosets preparation was as follows, with the formulations listed in Table S1 in Supplementary Information. Firstly, EP and DAL-*x* mixture was added to 15 mL of 1, 4-dioxane, stirred until completely dissolved, and then put in an oven to remove solvent at 105 °C. After cooling to 80 °C, DDM was added to the mixture and stirred until transparent. After defoaming in a vacuum for 5 min, the mixture was poured into the pre-heat mold, and the curing reaction was carried out firstly at 100 °C for 2 h and then at 150 °C for another 2 h. The cured samples were obtained after cooling to room temperature. The control samples were fabricated using the same conditions.

### 2.5. Characterizations

Fourier transform infrared spectroscopy (FTIR) was used to record the functional groups of both lignin and DAL-*x* on a Bruker Vector 22 FT-IR spectrometer as KBr pellets using 32 scans in the range of 4000–400 $cm^{-1}$. $^1H$ nuclear magnetic resonance ($^1H$ NMR) spectra were collected on a 400 MHz spectrometer (BRUKER AVANCE, Germany), in DMSO–$d_6$. Elemental analysis of DAL-*x* was performed on a Vario EL Cube element analyzer. Each sample was measured three times and the average value was obtained. Gel permeation chromatography (GPC) was used to determine the mean molecular weight ($M_n$), mass mean molecular weight ($M_w$), and dispersion ($Đ$) of DAL-*x* using a GPC1515 gel permeation chromatograph (Waters Inc., USA) with DMF as the solvent. Thermogravimetric analysis (TGA) tests were performed on a TASDTQ600 (TA Instruments, USA) thermogravimetric analyzer. Typically, about 8.0 mg of sample was heated from room temperature to 800 °C at a heating rate of 20 °C/min under nitrogen atmosphere.

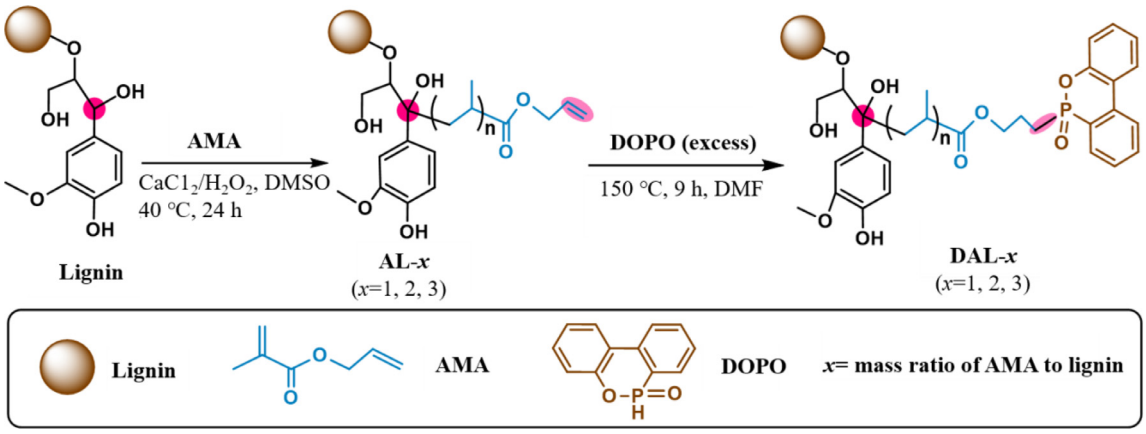


**Fig. 1.** Synthetic route of lignin-derived flame retardants (DAL-*x*).

LOI was measured on a JF-3 oxygen index meter (Jiangning, China) with sheet dimensions of 130 mm × 6.5 mm × 3 mm according to ISO4589-1984. The UL-94 rating was tested according to the ASTM D 63577 standard, and each sample dimension was 130 mm × 13 mm × 3.2 mm. The combustion behaviors of samples were evaluated on a cone calorimeter (CONE, FTT, UK) according to ISO 5660 with a heat incident flux of 35 kW/m$^2$. The sample dimension was 100 mm × 100 mm × 3.0 mm.

Dynamic mechanical analysis (DMA) was performed on a DMA Q800 apparatus (TA Instruments, USA) under single cantilever bending mode at a heat-up rate of 3 °C/min from 30 to 250 °C. The tensile properties were investigated using a CMT6000 universal mechanical testing machine (SANS, China) at a stretch speed of 5 mm/min according to the standard of GB/T 1040.1-2006. Five specimens were tested for each sample. A field emission scanning electron microscope (FEI-SEM, SU8010) was used to observe the dispersion of DAL-*x* within the EP matrix at an accelerating voltage of 3 kV. The fracture surface of DAL-*x*/EP composite was generated by quenching break in liquid nitrogen. Energy dispersive spectrometer (EDS) microanalyzer attached to FEI-SEM was applied to analyze the surface elemental composition of the sample.

Laser Raman spectroscopy (Raman, USA) was conducted using a 532 nm laser source with a wavenumber range of 100–800 cm$^{-1}$ on a Thermo Fischer DXR Raman microscope to measure the degree of graphitization of the char residue. The chemical compositions of residual chars were investigated using an ESCALAB XI + X-ray photoelectron (XPS) spectrometer (Thermo Fisher Scientific, USA) with Al $K_\alpha$ radiation. A real-time Fourier transform infrared (RT-FTIR) spectrophotometer (TGA4000+SP2, PE, USA) was employed to investigate the evolved char residues of EP thermosets during thermal oxidative degradation, which was equipped with a heating device. The gaseous decomposition products of EP samples were investigated by TGA coupled with FT-IR (TG-IR, PerkinElmer, USA). Acquisition interval was 2.24 s with a resolution of 4 cm$^{-1}$.

## 3. Results and discussion

### 3.1. Synthesis and characterization of DAL-x

Fig. 1 illustrates the synthetic route of DOPO-containing, lignin-derived flame retardants (DAL-*x*). Briefly, the synthesis process involves two steps, namely (1) the formation of the intermediate (AL-*x*, a functionalized lignin) by free radical polymerization between pristine lignin and allyl methacrylate (AMA), and (2) the production of the target DAL-*x* by the addition reaction between AL-*x* and DOPO.

The elemental distribution in Table S2 confirms the presence of phosphorus in DAL-*x* (5.05 wt.% for DAL-1, 4.03 wt.% for DAL-2, and 4.78 wt.% for DAL-3). Also, the GPC results (Table S3) of DAL-1, DAL-2 and DAL-3 show that they represent a series of oligomers, of which the $M_n$ and $Đ$ are 5524–7322 and 2.05–2.31, respectively. The increased $M_n$ and the fine polydispersity further demonstrate that DAL-*x* was successfully synthesized with good homogeneity.

The chemical structures of as-synthesized AL-3 and DAL-3 were characterized by FTIR. From Fig. 2(a), the FTIR spectrum of AMA shows characteristic peaks at 3085 (C–H), 1728 (–C=O), 1643 (C=C), 930 (–CH=CH$_2$), and 813 (C=C–H) cm$^{-1}$ [45]. For AL-3, the above characteristic peaks are also observed in its FTIR spectrum except for the C=C–H bond, indicating successful synthesis of AL-3. The FTIR spectrum of DAL-3 (Fig. 2(d)) shows some new peaks related to phosphorus-containing bonds, including those at 1242 and 937 cm$^{-1}$, which are assigned to P=O and P–O–C, respectively [46]. More importantly, the disappearance of the peaks at 2439 (P–H), 930 (–CH=CH$_2$), and 3085 (–CH=CH$_2$) cm$^{-1}$ in the FTIR spectrum of DAL-3 further confirms the successful addition between DOPO and AL-3.

The chemical structures of AL-3 and DAL-*x* were also confirmed by $^1$H NMR. For Fig. 2(b, e), the signals of $\delta$ = 1–4 ppm are belonging to methoxy proton on the benzene of lignin and aliphatic proton attached to benzene, respectively. In the $^1$H spectrum of AL-3 (Fig. 2(b)), the broad shift at $\delta$ = 6–8 ppm is corresponding to the protons on benzene rings of lignin, and those at $\delta$ = 5.25 (H-3), 5.32 (H-2), and 5.91 (H-1) ppm belong to different protons on –CH=CH$_2$ of AMA [47]. With the addition of DOPO, the disappearance of the alkene resonances at $\delta$ = 5.25 (H-3) and 5.32 (H-2) ppm indicates the addition reaction between AL-3 (–CH=CH$_2$) and DOPO (P-H). Additionally, the $^1$H NMR spectrum of DAL-3 also shows chemical shifts at $\delta$ = 6.80, 7.37, 7.77, and 8.20 ppm related to the protons on benzene rings of DOPO [23], further suggesting the successful addition of DOPO and AL-3.

The thermal stability of DAL-*x* was investigated using TGA under nitrogen (Fig. 2(c, f)). For pristine lignin, the first stage of thermal decomposition occurs at room temperature to 220 °C corresponding to the removal of moisture. After that, primary structure decomposition occurs in the temperature range of 220–400 °C, mainly due to the cleavage of functional groups and chemical linkages, such as methoxy, hydroxyl, carbonyl, C–C, and C–O–C, resulting in the generation of large amounts of gaseous products such as phenolics and other products (i.e. $H_2O$, $CO_2$, $CH_4$, and CO) [48,49]. From 400 to 800 °C, the re-condensation and rearrangement of aromatic rings happen, leading to the formation of lignin char with polyaromatic structures [50].

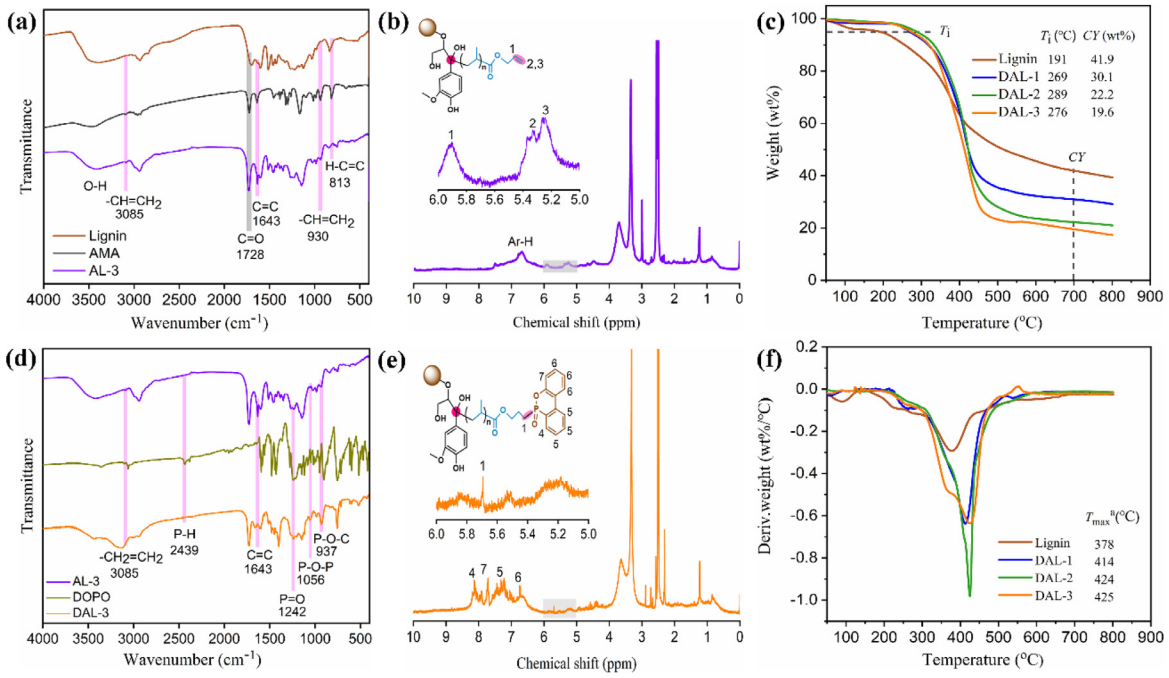


**Fig. 2.** (a, d) FTIR spectra of (a) pristine lignin, AMA, AL-3, DOPO, and DAL-3, (b, e) $^1$H NMR spectra of AL-3, and DAL-3, and (c, f) TG and DTG curves of DAL-*x* ($x$ = 1, 2, 3) under nitrogen atmosphere.

During the whole decomposition process, the initial decomposition temperature ($T_i$, the temperature of 5% mass loss), the maximum mass-loss-rate temperature ($T_{max}$), and the char yield (CY) at 700 °C are also critical parameters to evaluate thermal stability. For pristine lignin, the $T_i$, $T_{max}$, and CY are 191 °C, 378 °C, and 41.9 wt.%, respectively. After functionalization of AMA and then modification with DOPO, the $T_i$ of DAL-*x* obviously increases to 269 °C (DAL-1), 289 °C (DAL-2) and 276 °C (DAL-3), respectively. The $T_{max}$ value of DAL-1, DAL-2, and DAL-3 was 412, 424 and 425 °C, respectively, which is an increase of 34, 46 and 47 °C in comparison to that of pure lignin, indicating the enhanced thermal stability. The CY decreases (from 41.9 wt.% for pristine lignin to 19.6 wt.% for DAL-3), possibly due to the introduction of DOPO with the function of releasing gas-phase free radicals.

### 3.2. Screening of DAL-x as fire retardant for EP

UL-94 vertical burning and limiting oxygen index (LOI) tests are important for evaluating the flame retardancy of certain materials [51]. Fig. 3 shows the burning processes of EP samples, and the experimental data are presented in Table S4. As shown in Fig. 3(a), once ignited, the neat EP burns well with large amounts of smoke generated and fails to achieve any UL-94 rating. Unfortunately, the addition of 10 wt.% of AL-3 or 2 wt.% of DOPO failed to obviously improve the flame retardancy of EP (Table S4). With the addition of DAL-3, the burning of EP composites (e.g., 5DAL-3/EP and 7.5DAL-3/EP) is inhibited dramatically, with a noticeable decrease in burning time, leading to a UL-94 V-1 rating. When 10 wt.% of DAL-*x* (1/2/3) is added, the burning time of certain EP composites (i.e., 10DAL-*x*/EP) decreases significantly (< 10 s), and the UL-94 V-0 rating can be obtained.

From the perspective of LOI value (Table S4), the addition of DAL-*x* in EP increases these values (from 24.1% for EP to >27.9% for DAL-*x*/EP). Generally, a material with an LOI value > 26% can be categorized as a self-extinguishing material. Accordingly, the addition of DAL-*x* significantly improves the flame retardancy of EP. DAL-1 and DAL-2 exhibit higher efficiency than DAL-3 because both enable EP to self-extinguish within 5 s. After burning, lignin- and phosphorus-components can promote charring and dehydration to form a more continuous char layer with a denser structure, which can efficiently prevent the release of heat, volatiles, and smoke produced from EP combustion [43,44]. In the gas phase, the generation of PO• and $PO_2$• free radicals can effectively capture H• and •OH active radicals produced from EP combustion reactions to enhance the flame inhibition effect [52,53].

### 3.3. Thermal properties

TGA is used to evaluate the thermal stability and charring capability of EP and DAL-*x*/EP composites. As shown in Fig. 4(b, d), pure EP shows a single thermal decomposition step, including the breakage of C–C, aromatic C=C, C–O and C–N bonds [54], with a $T_i$ = 266 °C, a $T_{max}$ = 402 °C, a CY (800 °C) = 3.7 wt.%, and a $R_{max}$ = 34.03 wt.%/°C (Table S5). With the introduction of DAL-*x*, the thermal stability of these EP composites is improved significantly (Fig. 4(a, c)). For example, the $T_i$ values of 5DAL-3/EP and 10DAL-3/EP are both increased to 283 °C, which is 17 °C higher than that of pure EP, and the highest $T_i$ is obtained at 323 °C for 10DAL-1/EP. However, the $T_{max}$ of EP composites undergoes a decreasing trend. For example, as compared to pure EP, the $T_{max}$ of 10DAL-3/EP is reduced by 37 °C. Furthermore, the CY values at 800 °C of EP composites increase significantly, accompanied by a decreasing trend in $R_{max}$. For instance, the CY value of 10DAL-2/EP increases significantly to 19.4 wt.%, while the $R_{max}$ value decreases by 23.07 wt.%/°C relative to EP. The decrease of $R_{max}$ is associated with the enhanced char-forming capacity after the incorporation of DAL-*x* in EP. The increases in the initial thermal degradation temperature and char residue of EP composites are attributed to the disordered but rigid aromatic structure in DAL-*x*, which may improve the thermal stability of EP composites through intermolecular crosslinking.

The synergistic effect of lignin and phosphorus-containing components further enhances the charring capacity of EP [55]. However, the decreases of both $T_{max}$ and $R_{max}$ of EP composites may be due to the decomposition of phosphorous groups in advance, thus

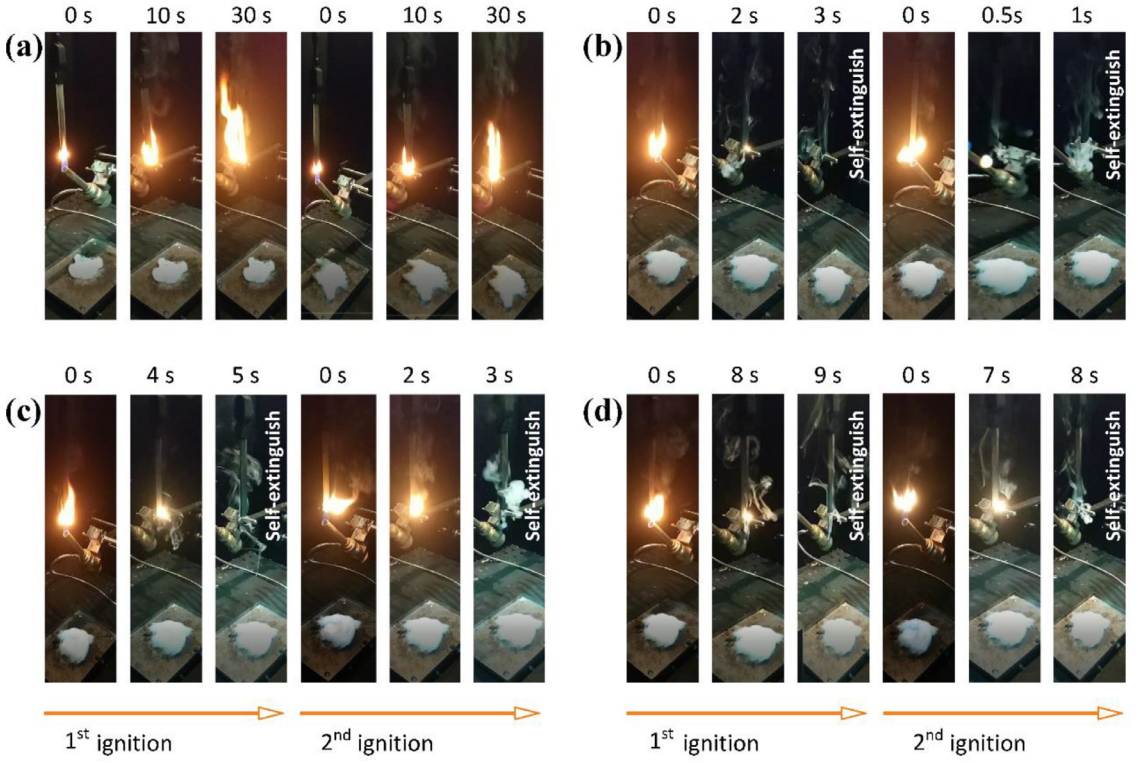


**Fig. 3.** Digital pictures of (a) EP, (b) 10DAL-1/EP, (c) 10DAL-2/EP, and (d) 10DAL-3/EP during UL-94 tests.

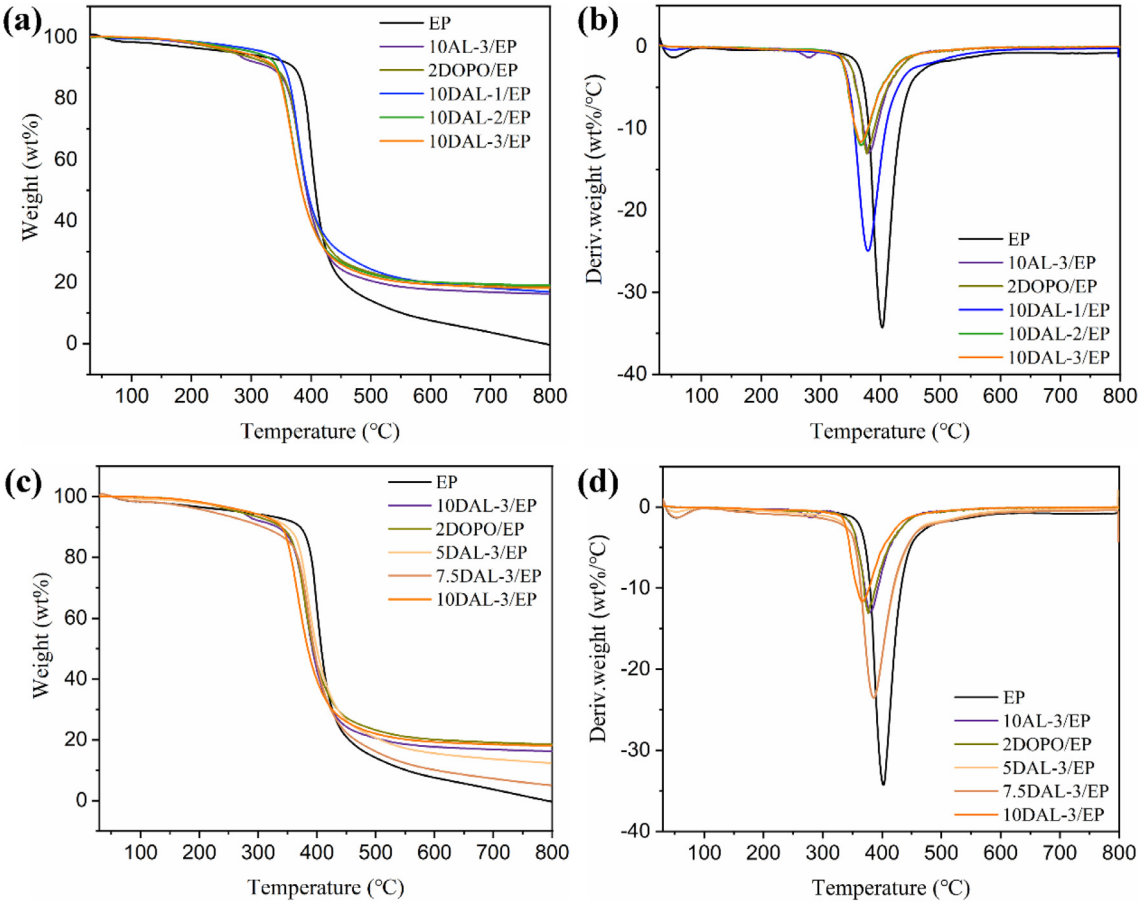


**Fig. 4.** (a, c) TG and (b, d) DTG curves of EP and EP composites under $N_2$ flow.

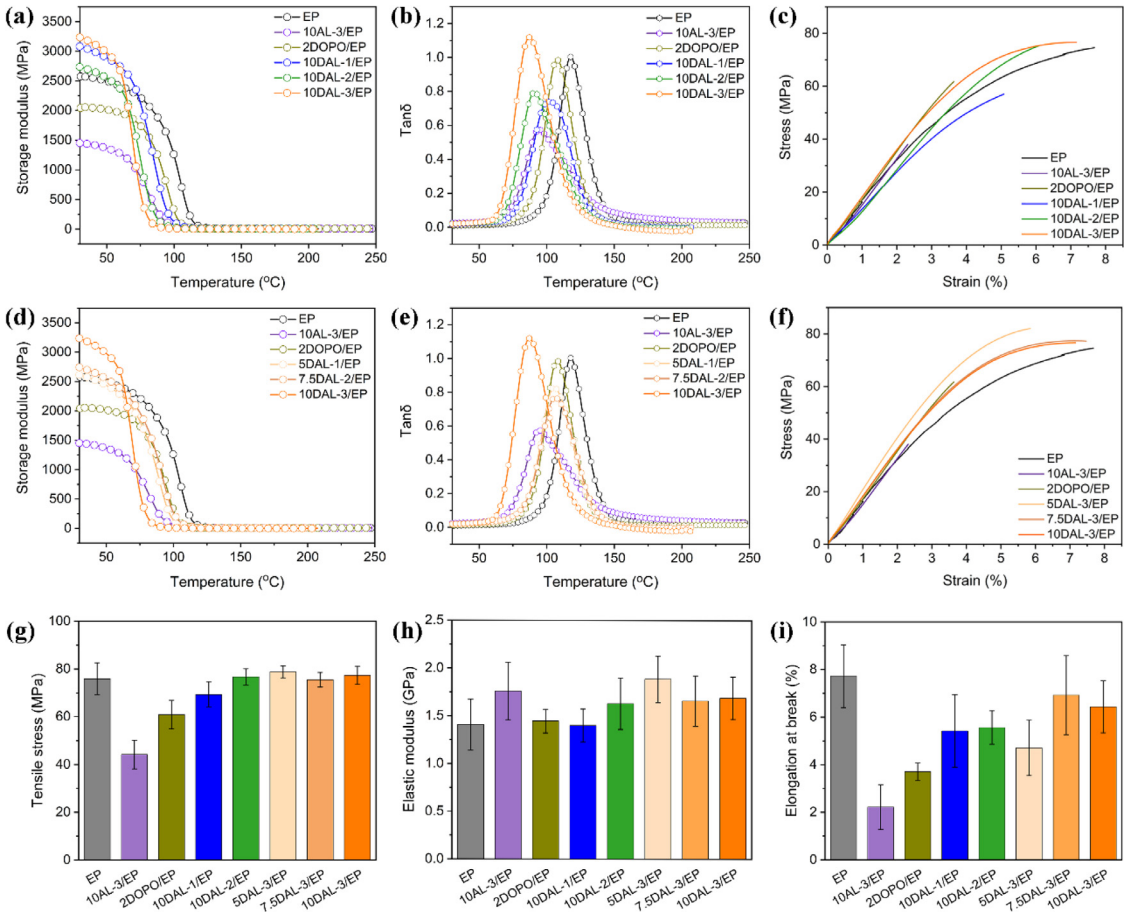


**Fig. 5.** (a, d) Storage modulus, (b, e) tan$\delta$, (c, f) tensile stress-strain curves, (g) tensile strength, (h) elastic modulus, and (i) elongation at break of EP and EP composites.

producing phosphoric acid, polyphosphate, and other acidic substances, which accelerate the structural decomposition of EP [24].

### 3.4. Dynamic and static mechanical properties

The impacts of DAL-*x* on the mechanical properties of EP thermosets are investigated by DMA and tensile tests, with the results shown in Fig. 5 and Table S6. Pure EP sample exhibits a high storage modulus ($E'$) of 2575 MPa at room temperature, with a relatively low glass transition temperature ($T_g$) of 117 °C. The introduction of 10 wt.% AL-3 or 2 wt.% DOPO fails to improve the thermomechanical properties of EP. Certain DAL-*x*/EP composites show increased $E'$ values at room temperature but decreased $T_g$ values. For example, the $E'$ values of 10DAL-1/EP, 10DAL-2/EP, and 10DAL-3/EP increase to 3080, 2732, and 3227 MPa at 25 °C, while their $T_g$ values decrease to 102, 90, and 87 °C (Table S6). In addition, the crosslinking density ($N$, mol/L) is related to the $T_g$ and $E'$, which can be calculated by Eq. (1):

$$N = E/3RT \quad (1)$$

where $E$, $R$ and $T$ respectively are the $E'$ at $T_g$ + 20 °C (MPa), the gas constant (8.314 L kPa $K^{-1}$ $mol^{-1}$) and absolute temperature (K) [55].

The $N$ of most EP composites increases with the introduction of lignin-derived flame retardants (Table S6), which is consistent with the enhancement in $E'$ of DAL-*x*/EP at room temperature. It may be attributed to the presence of rigid aromatic rings in DAL-*x*, which can fabricate stronger three-dimensional network in EP composites, further leading to the improvement in the stiffness (the higher elastic modulus) and tensile properties (the higher tensile strength) (Fig. 5(g, h)) [56]. However, the $N$ of 10DAL-3/EP decreases, which is probably because the addition of DAL-3 with large molecular weight increases the viscosity of the epoxy resin system. The high viscosity of the EP system is detrimental to the crosslinking reaction [57], resulting in incomplete curing and lower $N$ and $T_g$, thus deteriorating toughness (the lower elongation at break) (Fig. 5(i)).

To further study the influences of DAL-*x* on the mechanical properties of EP composites, the morphologies of fractural surfaces are observed using SEM in Fig. 6. The fractured surface of pure EP sample is relatively smooth with some linear cracks, indicating a typical brittle fracture character. The fractured surface of DAL-*x*/EP is rough with some small crinkles and ripples, indicating the increased fracture propagation path and area, which result in energy dissipation and promote toughness [30,58,59]. However, 5DAL-3/EP and 7.5DAL-3/EP fractural surfaces show few folds and inclined ripples, and more circular bulges, which is probably because the poor compatibility between DAL-3 and EP makes DAL-3 aggregate on the fractured surface, serving as some stress-concentration sites, accelerating fragile rupture and deteriorating mechanical performances (Fig. 6(d, e)) [46,60].

### 3.5. Flame retardancy

Cone calorimetry, a bench-scale fire testing method, has been widely used to assess the combustion behaviors of materials in a real fire scenario [61]. This is performed to further investigate the flame-retardant and smoke-suppressive performances of EP samples, with the curves and data shown in Fig. 7 and Table S7, respectively. Neat EP is ignited at 63 s with the highest PHRR and THR

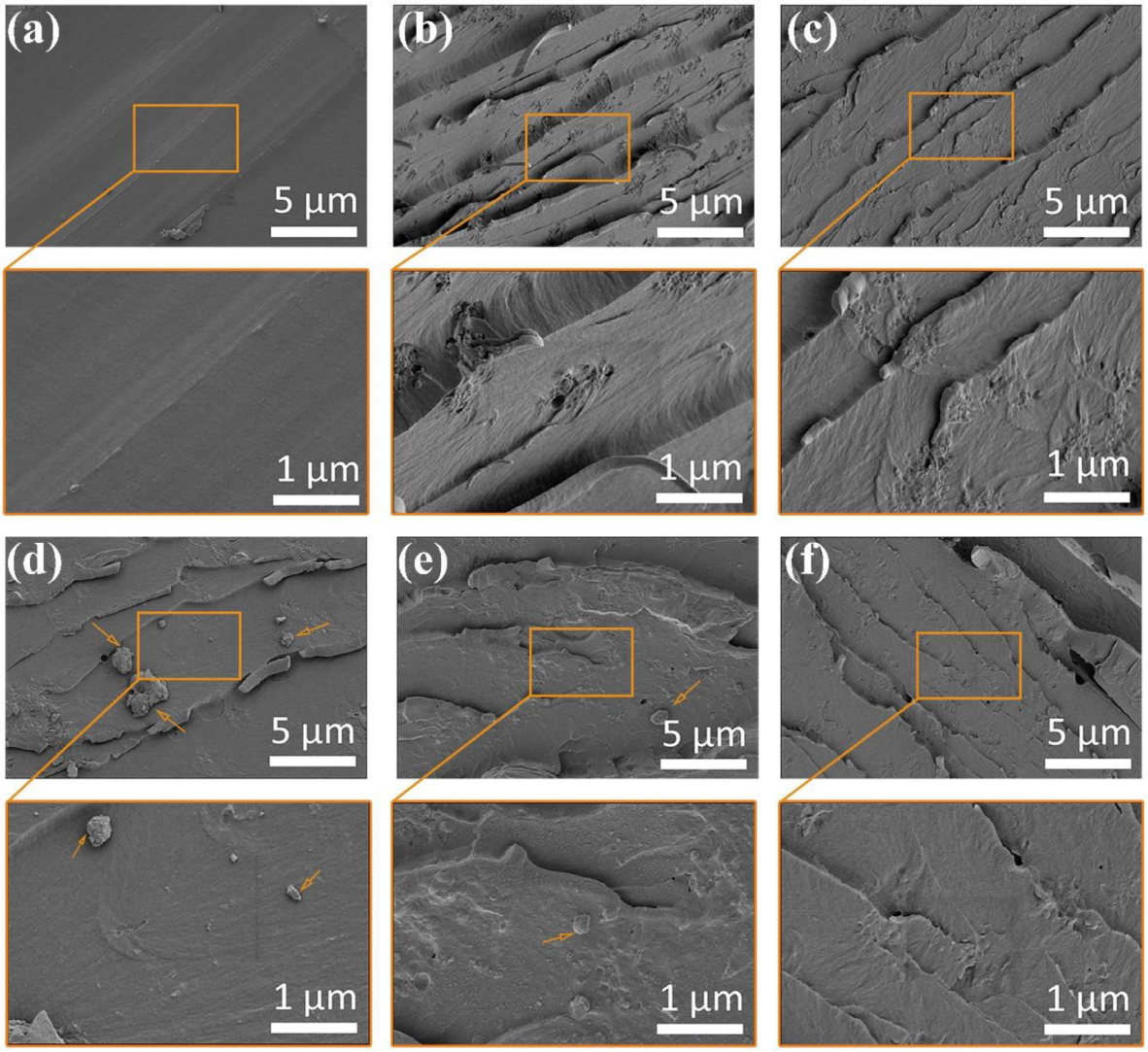


**Fig. 6.** SEM images of fracture surface morphologies for (a) EP, (b) 10DAL-1/EP, (c) 10DAL-2/EP, (d) 5DAL-3/EP, (e) 7.5DAL-3/EP, and (f) 10DAL-3/EP.

of 1240 kW/m$^2$ and 83 MJ/m$^2$ among all as-fabricated EP samples. With the introduction of DAL-*x*, the time to ignition (TTI) values of 10DAL-1/EP, 10DAL-2/EP, and 10DAL-3/EP are shortened to 47, 49, and 51 s, respectively. Additionally, DAL-*x*/EP samples exhibit significant reductions in PHRR and THR (Fig. 7(a, b, d, e)). For example, as compared to neat EP, the PHRR value of 10DAL-2/EP decreases by about 24%, and the THR value of 10DAL-1/EP decreases by about 22%. Although 7.5DAL-3/EP fails to reach V-0 rating in the UL-94 test, the reduced PHRR and THR values also show its excellent flame retardancy. In comparison to 10AL-1/EP, better flame retardancy can be obtained on DAL-*x*/EP composites, owing to the synergistic effect of lignin and phosphorus-containing components. It is worth noting that the DAL-*x* as a flame retardant is more excellent in the reduction of the both PHRR and THR for EP composites than many previously reported lignin-based flame retardants/EP composites (Fig. S1 in Supplementary Information) [24,25,28,44,46,62–64].

For smoke generation during combustion, among all EP samples, virgin EP with the highest flammability causes the most smoke generation on burning, of which the peak of smoke production rate (PSPR) and TSP reach 0.364 m$^2$/s and 32.3 m$^2$, respectively. With the introduction of DAL-*x*, the obtained EP composites exhibit smoke suppression. For instance, the PSPR values of 10DAL-3/EP and 10DAL-2/EP decrease by about 21% and 15% (Table S7), respectively. The addition of DAL-*x* also causes a significant increase in residual weight (RW) of EP composite by 81%–143%, showing its usefulness in promoting charring capacity. Also, the increased char residue promotes the formation of a continuous compact char layer on the surface of EP matrix, effectively inhibiting the combustion of matrix, and reducing the smoke release. With DAL-*x* addition, the fire performance index (FPI) of EP composites increases with the fire growth index (FGI) decreasing. FPI and FGI are important indexes to evaluate the fire safety of materials, the higher FPI and/or the lower FGI, suggesting the higher fire safety [65]. Hence, DAL-*x* does improve the fire safety of EP, especially in the enhancement of smoke suppression.

In addition, the comprehensive flame retardant properties of EP composites were studied by calculating the flame inhibition effect, charring effect and barrier effect [66].

$$\text{Flame inhibition effect} = \left(1 - \frac{\text{EHC}_{\text{DAL}-x}}{\text{EHC}_{\text{pure}}}\right) \times 100\% \quad (2)$$

$$\text{Charring effect} = \left(1 - \frac{\text{TML}_{\text{DAL}-x}}{\text{TML}_{\text{pure}}}\right) \times 100\% \quad (3)$$

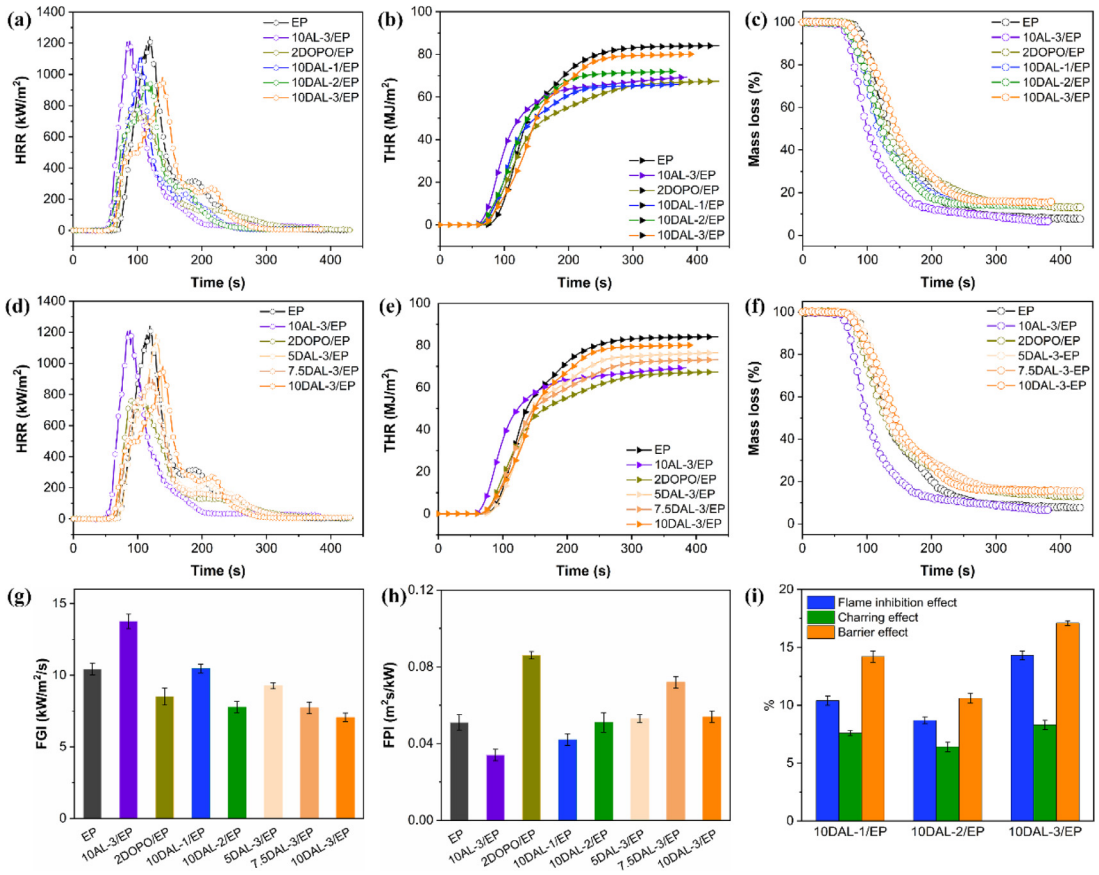


**Fig. 7.** (a, d) Heat release rate (HRR), (b, e) total heat release (THR), (c, f) total mass loss curves (Mass loss), (g) fire growth index (FGI) curves, (h) fire performance index (FPI) curves of EP and EP composites, and (i) corresponding flame-retardant effects.

$$\text{Barrier effect} = \left(1 - \frac{\frac{\text{PHRR}_{\text{DAL}-x}}{\text{PHRR}_{\text{pure}}}}{\frac{\text{THR}_{\text{DAL}-x}}{\text{THR}_{\text{pure}}}}\right) \times 100\% \quad (4)$$

where TML presents total mass loss, DAL-*x* presents DAL-*x*/EP, and pure presents EP. Finally, the comprehensive flame-retardant properties of EP composites are shown in Fig. 7(i), which highlight the excellent charring and flame inhibition effects of DAL-*x*, and the best performance can be obtained on 10DAL-3/EP.

Previous studies have shown that phosphorus-containing, lignin-based flame retardants mainly play an important role in the condensed phase of EP during burning [61]. For this purpose, the macro- (Fig. S2) and micro-morphologies (Fig. 8) of char layers for EP and DAL-*x*/ EP samples after cone calorimeter tests were investigated. At the macro scale, pure EP almost burns out after the test, leaving only a fragile residue layer with large holes on the surface, and the char height is only 0.4 cm (Fig. S1(a)). With the incorporation of DAL-*x*, the content of residual char increases significantly and has better structural integrity (Fig. S1(b–f)). For example, as flame retardant is added, the height of residual char of 10DAL-1/EP, 10DAL-2/EP, and 10DAL-3/EP significantly increases by 5, 4.5 and 3.75 times (compared with 0.4 cm of EP) to 2, 1.8, and 1.5 cm, respectively.

At the micro-scale, certain cracks appear on the surface of pure EP (Fig. 8(a)), while with the addition of DAL-*x*, cracks on the char surface of EP composites are reduced, and the char layer becomes more continuous and denser (Fig. 8(b–d)). The intumescent char layer can effectively block the transfer of heat, oxygen, and combustible species, showing a strong barrier effect towards flames. The introduction of DAL-*x* promotes the formation of convex structures inside the char layer of EP composites (marked by the yellow arrows in Fig. 8(b, c)), which can store large quantities of phosphorous fragments and non-flammable gases. When the internal gas pressure is enough to break through the residual char layer, the phosphorous free radicals are released immediately and quench the flame. Also, the release of non-flammable gases dilutes oxygen concentration, thus suppressing the burning reaction [52,67]. The EDS mapping results further reveal that the high-quality char layer is closely related to the participation of phosphorous components [68]. In conclusion, phosphorous promotes the formation of a compact and dense char layer during epoxy combustion, decelerating heat transfer and protecting the underlying matrix from further combustion [69].

### 3.6. Condensed phase

The chemical components of residual chars for EP and DAL-*x*/EP samples after cone calorimeter tests are studied by Raman and XPS techniques, with the spectra shown in Fig. 9. As shown in Fig. 9(a, b), Raman spectra show D- and G-type bands, located at 1350 and 1600 $cm^{-1}$, which are disordered carbon and graphite carbon vibrations, respectively [70]. The integral area ratio of D and G bands ($I_D/I_G$) manifests the degree of graphitization and thermal stability of char residue. The lower the $I_D/I_G$ ratio, the higher the degree of graphitization, and the better the thermal stability [71]. The $I_D/I_G$ value of EP residue is 3.53, higher than that of 10DAL-3/EP char (3.29), which indicates that the introduction of DAL-*x* improves the graphitization degree of the char residue, thus leading to the enhanced flame retardancy in condensed phase.

Fig. 9(c–f) displays the XPS spectra of residual chars for EP and 10DAL-3/EP composite. Phosphorus only remaining in the residual

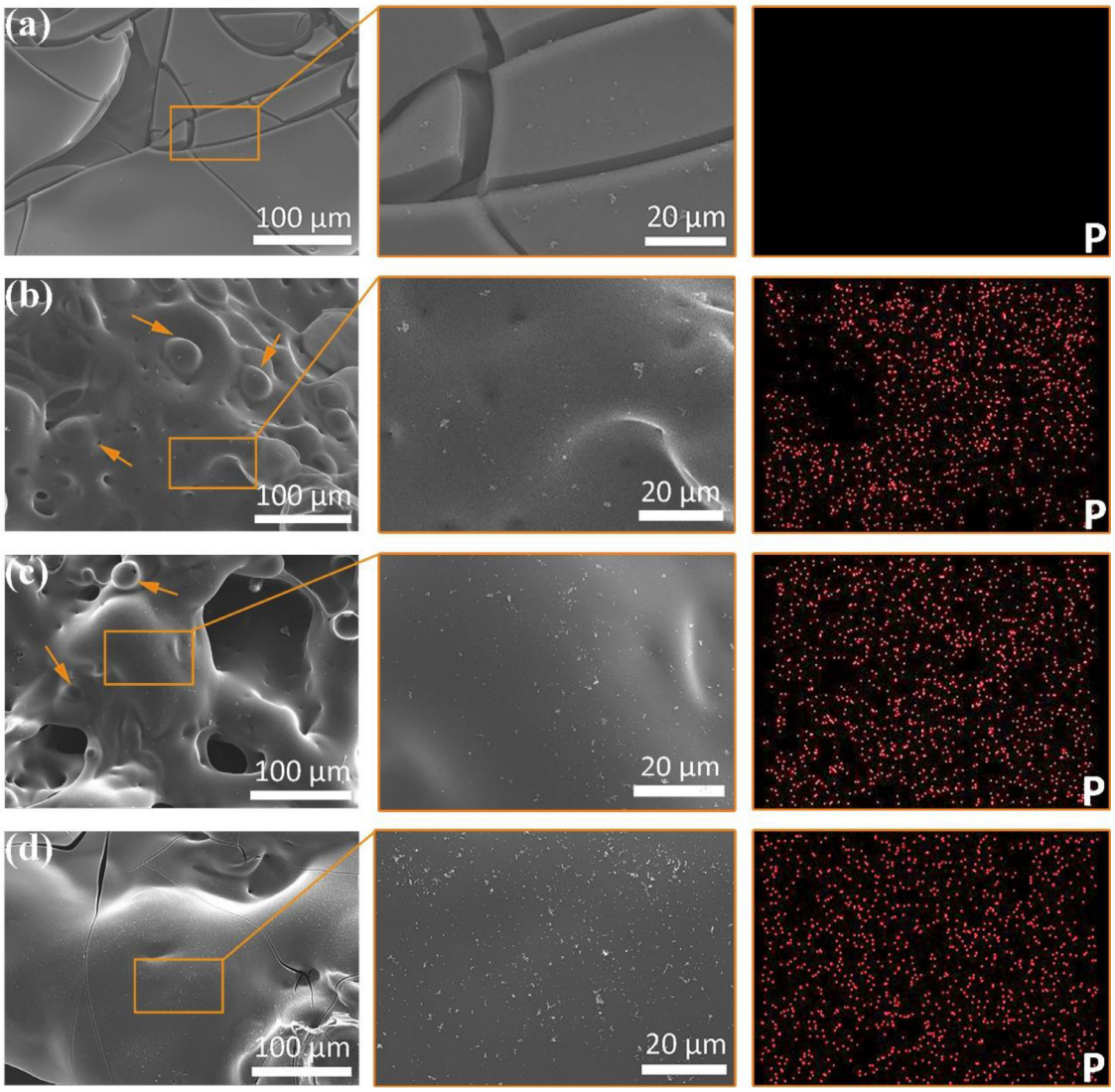


**Fig. 8.** SEM images and P-element mapping image of char residues for EP and EP composites after cone calorimeter tests: (a) EP, (b) 10DAL-1/EP, (c) 10DAL-2/EP, and (d) 10DAL-3/EP.

char of 10DAL-3/EP (Fig. 9(c)) can play a critical role in condensed-phase flame retardancy. The high-resolution XPS spectra of 10DAL-3/EP in C 1s, O 1s, and P 2p regions are displayed in Fig. 9(d–f). The C 1s spectrum of 10DAL-3/EP is fitted to three deconvoluted peaks (C=C/C–C, C–O, and C=O peaks at 284.7, 285.8, and 289.1 eV, respectively) [26]. In terms of O 1s spectrum, two deconvoluted peaks at 532.8 and 533.5 eV are assigned to C=O and C–O, respectively [72]. Additionally, two deconvoluted peaks of P–O and P–C at 135.4 and 133.5 eV are fitted in Fig. 9(f) [73], indicating that the phosphate groups in 10DAL-3/EP participate in the char formation through a crosslinking reaction, thus improving the barrier properties in the condensed phase [74].

### 3.7. TG-IR

Thermal degradation of polymers involves various complex reactions, such as chain termination, radical formation, and generation of various thermal cracking products, which directly affect combustion behaviors. To further evaluate the influence of DAL-*x* on the combustion process of EP, the TG-IR was used to study the gaseous product generation by thermal degradation of EP and EP composites. The characteristic absorption peaks of neat EP can be observed at 3653 (O–H), 2886–3043 (hydrocarbons), 1611, 1510, 749 (carbonyl compounds), and 1259 and 1175 (aliphatic ethers) $cm^{-1}$ (Fig. 10(a, d, e)) [75]. The main volatile products of 10DAL-3/EP are basically the same as those of pure EP, while the main difference is that the intensity of the C=O peak (1755 $cm^{-1}$) of 10DAL-3/EP is much weaker than that of pure EP, indicating that the introduction of DAL-*x* inhibits the generation of combustible carbonyl compounds. From Fig. 10(a), at $T_{max}$, the addition of DAL-*x* reduces the generation of all volatiles, highlighting its gas inhibition effect, which can be attributed to the charring capacity of lignin and the quenching factors (PO•, $PO_2$•) derived from DOPO components, corresponding to the result obtained from many studies [44,63].

Fig. 10(b, c) shows the RT-FTIR spectra of EP substrates at 30–600 °C, while the main decomposition process happens at 300–400 °C (as seen in Fig. 10(d, e)). Such results validate that DAL-3 in the condensed phase enhances the thermal resistance of the char layer and fire safety of EP by promoting the formation of residual char with a polyaromatic structure and thermally stable properties. As mentioned previously, lignin promotes the formation

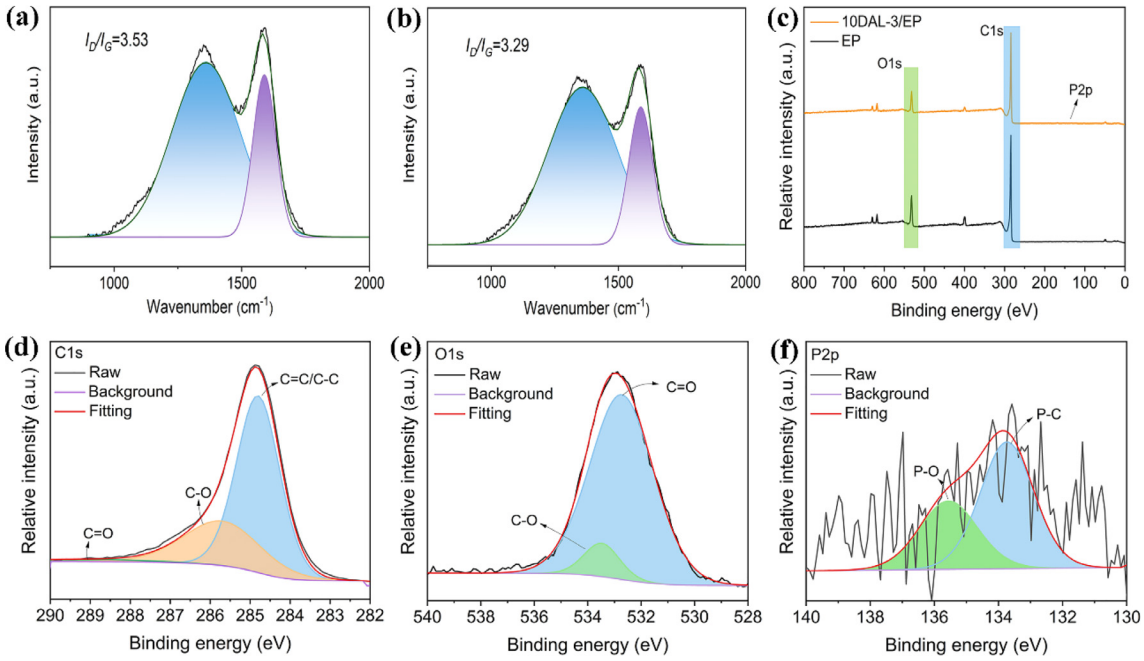


**Fig. 9.** Raman spectra of residual chars for (a) EP and (b) 10DAL-3/EP, (c) full-scan XPS spectra of residual chars for EP and 10DAL-3/EP, and (d) C 1s, (e) O 1s, and (f) P 2p high-resolution XPS spectra of char for 10DAL-3/EP.

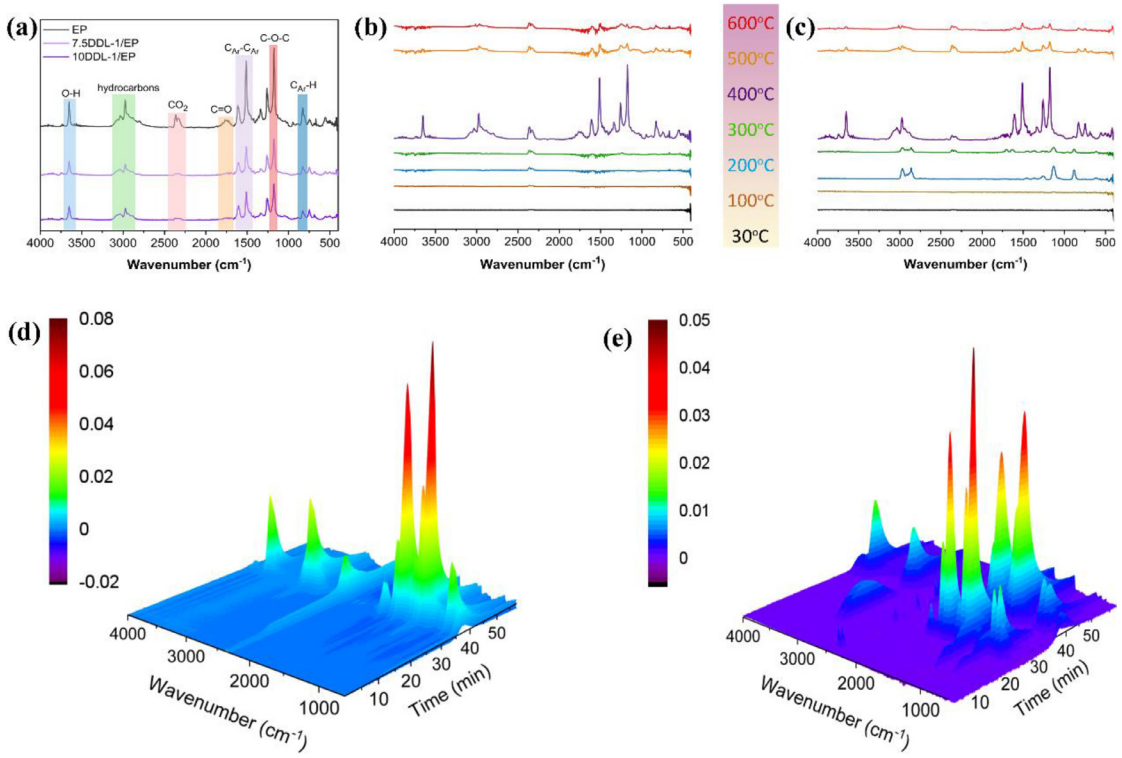


**Fig. 10.** (a) TG-IR spectra of EP and 10DAL-3/EP at $T_{max}$ in $N_2$ conditions, RT-FTIR spectra of (b) EP and (c) 10DAL-3/EP at different temperatures in $N_2$ conditions, and 3D TG-IR spectra of (d) EP and (e) 10DAL-3/EP in $N_2$ conditions.

of polyaromatic structures during the thermal decomposition of EP, resulting in more residual char generation [46,76]. During the decomposition of phosphorus components, phosphate-based free radicals are generated, which effectively capture active free radicals generated by the combustion of EP, realizing fire quenching and reducing the release of combustible materials, thereby improving flame retardancy.

## 4. Conclusion

In this work, a novel series of bio-based flame retardants were synthesized by grafting DOPO onto lignin through free radical copolymerization and addition reaction, which was used to fabricate high-performing EP composites. As little as 10 wt.% DAL-*x* endows DAL-*x*/EP composite with desired flame retardancy (including a UL-

94 V-0 rating and an LOI of 29.8%), accompanied by 24% and 21% reductions in PHRR and PSPR relative to pure EP. The excellent fire safety of DAL-*x*/EP composites is attributed to the quenching and charring effects derived from DAL-*x*. The phosphorus components (PO• and $PO_2$• radicals) derived from DAL-*x* capture H• and OH• radicals formed by EP combustion, thus quenching the fire. Additionally, the lignin of DAL-*x* promotes char-formation to reduce the release of volatiles and enhances the density and strength of the char layer. Furthermore, 10DAL-3/EP composite has robust mechanical properties with an enhanced elastic modulus (1.7 GPa), well-preserved tensile strength (77.3 MPa) and breaking elongation (6.4%), due to good dispersion and interfacial compatibility. This study provides an effective method for preparing highly efficient lignin-based flame retardants with multiple functions, which is expected to promote the development of lignin-based flame retardants in the future and is more conducive to improving lignin valorization.

## Declaration of Competing Interest

The authors declare that they have no known competing financial interests or personal relationships that could have appeared to influence the work reported in this paper.

## Acknowledgments

This work was financially supported by the National Natural Science Foundation of China (Nos. 51873196 and 51903222), the Australian Research Council (Nos. LP220100278, DP190102992 and FT190100188), the Natural Science Foundation of Zhejiang Province (No. LY21E030001), and the “Pioneer” and “Leading Goose” R&D Program of Zhejiang (No. 2022C03128).

## Supplementary materials

Supplementary material associated with this article can be found, in the online version, at doi:10.1016/j.jmst.2023.06.004.

## References

[1] Q.Q. Luo, Y.L. Sun, B. Yu, C.P. Li, J.L. Song, D.X. Tan, J.Q. Zhao, Polym. Degrad. Stab. 165 (2019) 137.
[2] Y.Y. Fang, L.J. Qian, Z.G. Huang, S. Tang, Y. Qiu, RSC Adv. 7 (2017) 46505.
[3] X.W. Li, T. Shi, B. Li, C.W. Zhang, Z.G. Guo, Q.X. Zhang, Mater. Des. 183 (2019) 108152.
[4] M.J. Cui, S.M. Ren, H.C. Zhao, Q.J. Xue, L.P. Wang, Chem. Eng. J. 335 (2018) 255–266.
[5] J. Wang, Y.S. Liu, X.Y. Guo, H.Q. Qu, R. Chang, J. Ma, ACS Omega 5 (2020) 32286-32284.
[6] R. Haney, R.H. Kollarigowda, L. Wiegart, S. Ramakrishnan, ACS Appl, Nano Mater. 5 (2022) 1891–1901.
[7] Y. Jiang, J. Yun, X.C. Pan, ACS Sustain. Chem. Eng. 10 (2022) 16555–16562.
[8] Z.P. Cheng, M.H. Fang, X.X. Chen, Y.T. Zhang, Y.X. Wang, H.J. Li, J. Q, ACS Omega 5 (2020) 4200–4212.
[9] T.Y. Wang, G.X. Zhang, B.Y. Zhang, S.M. Liu, D.Y. Li, C. Liu, ACS Appl. Nano Mater. 4 (2021) 4153–4161.
[10] S.Q. Huo, J. Wang, S. Yang, X. Chen, B. Zhang, Q.L. Wu, B. Zhang, Polym. Advan. Technol. 29 (2017) 497–506.
[11] F.H. Yang, X. Zhang, Z.H. Yao, ACS Appl. Electron. Mater. 4 (2022) 1891–1900.
[12] Y.L. Sang, Q. Liu, S.X. Wang, S.H. Dong, Y.Z. Fan, X. Zhao, S.J. Li, Appl. Surf. Sci. 592 (2022) 153229.
[13] M. Kamran, A.H.A. Shah, G. Rahman, S. Bilal, P. Röse, Polymers-Basel 14 (2022) 5128.
[14] F. Liu, G.F. Jiang, X.X. Zhao, W. Li, Y.L. Che, China Pet. Process. Petrochem. Technol. 23 (2021) 109–120.
[15] X. Zhou, S.L. Qiu, X.W. Mu, M.T. Zhou, W. Cai, L. Song, W.Y. Xing, Y. Hu, Compos. Pt. B-Eng. 202 (2020) 108397.
[16] Y.Z. Fang, J.S. Miao, X.W. Yang, Y. Zhu, G.Y. Wang, Chem. Eng. J. 385 (2020) 123830.
[17] Y.F. Ai, F.Q. Pang, Y.L. Xu, R.K. Jian, Ind. Eng. Chem. Res. 59 (2020) 11918–11929.
[18] S.G. Wang, B. Yu, K.Q. Zhou, L. Yin, Y. Zhong, X. Ma, J. Colloid. Interface Sci. 550 (2019) 210–219.
[19] J.F. Cui, B.Y Chen, J.H. Guo, Y.J. Zhou, B.P. Yang, Appl. Mech. Mater. 275-277 (2013) 1921–1924.
[20] Z.J. Wu, S.C. Li, M.J. Liu, H.Y. Wang, Z. Wang, X. Liu, Polym. Adv. Technol. 27 (2016) 98–108.
[21] B.W. Liu, H.B. Zhao, Y.Z. Wang, Adv. Mater. 34 (2022) 2107905.
[22] X. Zhong, X.T. Yang, K.P. Ruan, J.L. Zhang, H.T. Zhang, J.W. Gu, Macromol. Rapid Commun. 43 (2022) 2100580.
[23] T. Sai, S.Y. Ran, Z.H. Guo, H.Q. Yan, Y. Zhang, H. Wang, P.A. Song, Z.P. Fang, Chem. Eng. J. 409 (2021) 128223.
[24] H. Wang, Q. Liu, X. Zhao, Z. Jin, Poly. Degrad. Stab. 183 (2021) 109440.
[25] X.X. Wang, W.T. He, L.J. Long, S.W. Huang, S.H. Qin, G.M. Xu, J. Therm. Anal. Calorim. 145 (2021) 331–343.
[26] R. Chen, K.X. Hu, H. Tang, J.J. Wang, F.S. Zhu, H. Zhou, Polym. Degrad. Stab. 166 (2019) 334–343.
[27] J. Gao, W.J. Huang, W.T. He, L.J. Long, S.H. Qin, J. Therm. Anal. Calorim. 147 (2022) 1265–1274.
[28] J. Koedel, C. Callsen, M. Weise, F. Puchtler, A. Weidinger, V. Altstaedt, R. Schobert, B. Biersack, Polym. Test. 90 (2020) 106702.
[29] S.J. Jin, L.J. Qian, Y. Qiu, Y.J. Chen, F. Xin, Polym. Degrad. Stab. 166 (2019) 344–352.
[30] X.F. Liu, Y.F. Xiao, X. Luo, Chem. Eng. J. 427 (2022) 132031.
[31] L.N. Liu, M.B. Qian, P.A. Song, G.B. Huang, Y.M. Yu, S.Y. Fu, ACS Sustain. Chem. Eng. 4 (2016) 2422–2431.
[32] L.N. Liu, G.B. Huang, P.A. Song, Y.M. Yu, S.Y. Fu, ACS Sustain. Chem. Eng. 4 (2016) 4732–4742.
[33] T.B. Ma, H. Ma, K.P. Ruan, X.T. Shi, H. Qin, S.Y. Gao, J.W. Gu, Chin. J. Polym. Sci. 40 (2022) 248–255.
[34] R. Zhang, X.F. Xiao, Q.L. Tai, H. Huang, Y. Hu, Polym. Eng. Sci. 52 (2012) 2620–2626.
[35] M. Canetti, F. Bertini, A. De Chirico, G. Audisio, Polym. Degrad. Stab. 91 (2006) 494–498.
[36] A. Cayla, F. Rault, S. Giraud, F. Salaün, R. Sonnier, L. Dumazert, Materials 12 (2019) 1146.
[37] M.Y. Zhi, Q.Y. Liu, H. Chen, X.T. Chen, S.H. Feng, Y.H. He, ACS Omega 4 (2019) 10975–10984.
[38] K. Wang, H. Liu, C. Wang, W.J. Huang, T. Qin, Q.P. Fu, W. Yan, ACS Omega 6 (2021) 666–674.
[39] M.H. Fang, J. Qian, X.Z. Wang, Z Chen, R.L. Guo, Y.F. Shi, ACS Omega 6 (2021) 7094–7105.
[40] J.J. Wang, H. Zhou, Z.Q. Pan, H.J. Wu, D.S. Wang, Polym. Adv. Technol. 33 (2022) 1533–1543.
[41] M.C. Li, Y. Wang, C.H. Shen, S.J. Gao, J. Elastom. Plast. 54 (2022) 209–224.
[42] X.H. Shi, Q.Y. Liu, X.L. Li, A.K. Du, J.W. Niu, Y.M. Li, Z. Zhi, M. Wang, D.Y. Wang, Polym. Degrad. Stab. 197 (2022) 109839.
[43] X.Y. Lu, X.J. Zhu, P. Dai, H.M. Robin, H.Q. Guo, H. Que, D.D. Wang, D.X. Liang, T. He, C.Z. Xu, Z.Y. Luo, X.L. Guo, J. Therm. Anal. Calorim. 147 (2022) 5237–5253.
[44] X.Y. Lu, X.L. Gu, Int. J. Biol. Macromol. 205 (2022) 539–552.
[45] H.J. Yang, X.L. Qian, W.Y. Huang, X.Q. Xue, B.B. Jiang, Acta Polym. Sin. 5 (2015) 550–555.
[46] L.N. Liu, B.B. Shi, A.L. Zhang, Y.J. Xue, J.Z. Zhang, J.F. Dai, M. Hassanpour, L.C. Tang, Y.Q. Shi, P.A. Song, Compos. Pt. A-Appl. Sci. Manuf. 160 (2022) 107028.
[47] H.J. Yang, T. Bai, X.Q. Xue, W.Y. Huang, J.H. Chen, X.L. Qian, G.Z. Zhang, B.B. Jiang, Polymer 72 (2015) 63–68.
[48] M. Zhang, F.L.P. Resende, A. Moutsoglou, D.E. Raynie, J. Anal. Appl. Pyrol. 98 (2012) 65–71.
[49] D.K. Shen, G.F. Liu, J. Zhao, J.T. Xue, S.P. Guan, R. Xiao, J. Anal. Appl. Pyrol. 112 (2015) 56–65.
[50] Z.Q. Ma, J.H. Wang, H.Z. Zhou, Y. Zhang, Y.Y. Yang, X.H. Liu, J.W. Ye, D.Y. Chen, S.R. Wang, Fuel Process. Technol. 181 (2018) 142–156.
[51] Z.W. Ma, X.C. Liu, X.D. Xu, L. Liu, B. Yu, C. Maluk, G.B. Huang, H. Wang, ACS Nano 15 (2021) 11667–11680.
[52] N. Teng, J.Y. Dai, S.P. Wang, J.Y. Hu, X.Q. Liu, Chem. Eng. J. 428 (2022) 131226.
[53] Y.X. Yang, Z. Li, G. Wu, W. Chen, G.Y. Huang, Polym. Degrad. Stab. 196 (2022) 109841.
[54] W.T. He, P.A. Song, B. Yu, Z.P. Fang, H. Wang, Prog. Mater. Sci. 114 (2020) 100687.
[55] J.K. Liu, J.Y. Dai, S.P. Wang, Y.Y. Peng, L.J. Cao, X.Q. Liu, Compos. Pt. B-Eng. 190 (2020) 107926.
[56] S.Q. Huo, Z.X. Zhou, J.W. Jiang, T. Sai, S.Y. Ran, Z.P. Fang, P.A. Song, H. Wang, Chem. Eng. J. 427 (2022) 131578.
[57] X.N. Lu, M. Yu, D. Wang, P.C. Xiu, C.Z. Xu, A.F. Lee, X.L. Gu, Mater. Today Chem. 22 (2021) 100562.
[58] J.J. Lin, S.H. Bang, M.H. Malakooti, H.A. Sodano, ACS Appl. Mater. Interfaces 9 (2017) 11167–11175.
[59] R.K. Jian, X.B. Lin, Z.Q. Liu, W. Zhang, J. Zhang, L. Zhang, Z. Li, D.Y. Wang, Compos. Pt. B-Eng. 200 (2020) 108349.
[60] X.D. Xu, J.F. Dai, Z.W. Ma, L.N. Liu, X.H. Zhang, H.Z. Liu, L.C. Tang, G.B. Huang, H. Wang, P.A. Song, Compos. Pt. B-Eng. 190 (2020) 107930.
[61] S. Yang, S.Q. Huo, J. Wang, B. Zhang, J.S. Wang, S.Y. Ran, Z.P. Fang, P.A. Song, H. Wang, Compos. Pt. B-Eng. 207 (2021) 108601.
[62] Y. Wei, S.Y. Zhu, Q.W. Qian, L.Y. Liu, K.J. Jin, W.S. Liu, Y.P. Qiu, Ind. Crop. Prod. 187 (2022) 115543.
[63] X. Lu, A.F. Lee, X.L. Gu, Mater. Today Chem. 26 (2022) 101184.
[64] X.Y. Lu, X.L. Gu, Ind. Crop. Prod. 192 (2023) 116151.
[65] S.Q. Huo, S. Yang, J. Wang, J.W. Cheng, Q.Q. Zhang, Y.F. Hu, G.P. Ding, Q.X. Zhang, P.A. Song, H. Wang, ACS Appl, Polym. Mater. 2 (2020) 3566–3575.

[66] T. Shuo, W. Volker, K. Patrick, Q.L. Jun, Y.P. Qian, B. Schartel, RSC Adv. 7 (2017) 720–728.
[67] H.W. Qiao, L.P. Su, C.P. Liu, H.G. Zhang, M.F. Chen, Polym. Adv. Technol. 33 (2022) 1695–1705.
[68] Y.J. Xue, J.B. Feng, Z.W. Ma, L.N. Liu, Y. Zhang, J.F. Dai, Z.Q. Xu, S. Bourbigot, H. Wang, P.A. Song, Mater. Today Phys. 21 (2021) 100568.
[69] C. Liu, K. Xu, Y.Q. Shi, J.W. Wang, S.N. Ma, Y.Z. Feng, Y.C. Lv, F.Q. Yang, M.H. Liu, P.A. Song, Mater. Today Phys. 22 (2022) 100607.
[70] J. Zhang, Z. Li, L. Zhang, Y.X. Yang, D.Y. Wang, ACS Sustain. Chem. Eng. 8 (2020) 994–1003.
[71] B. Yu, A.C.Y. Yuen, X.D. Xu, Z.C. Zhang, W. Yang, H.D. Lu, B. Fei, G.H. Yeoh, P.A. Song, H. Wang, J. Hazard Mater. 401 (2021) 123342.
[72] X.W. Yang, L. Zhao, F. Peng, Y. Zhu, G.Y. Wang, Polym. Degrad. Stab. 193 (2021) 109721.
[73] J.W. Wang, S.L. Qiu, L. Cheng, W.J. Chen, Y.F. Zhou, B. Zou, L.F. Han, Z.M. Xu, W.H. Yang, Y. Hu, L. Song, Appl. Surf. Sci. 571 (2022) 151356.
[74] H.T. Yang, B.B. Shi, Y.J. Xue, Z.W. Ma, L.N. Liu, L. Lei, Y.M. Yu, Z.Y. Zhang, P.K. Annamalai, P.A. Song, Biomacromolecules 22 (2021) 1432–1444.
[75] X.D. Qian, L. Song, B. Yu, B.B. Wang, B.H. Yuan, Y.Q. Shi, Y. Hu, R.K.K. Yuen, J. Mater. Chem. A 1 (2013) 6822–6830.
[76] H.T. Yang, B. Yu, X.D. Xu, S. Bourbigot, H. Wang, P.A. Song, Green Chem. 22 (2020) 2129–2161.